Tow-Body Control System Modeling and Tuning on a Real-World Vehicle

Jasmine (Cashbaugh) Droppers
Control Systems Engineer
Kraken Robotic Systems
Dartmouth, Canada
jdroppers@krakenrobotics.com

Wesley Fisher
Software Developer
Kraken Robotic Systems
Dartmouth, Canada
wfisher@krakenrobotics.com

Andriy Predmyrskyy
Control System Engineer
Kraken Robotic Systems
Dartmouth, Canada
apredmyrskyy@krakenrobotics.com

***Abstract*—This paper presents a model-based approach for developing a stable, robust control system for a shallow water survey towfish. A model of the towfish system was developed based on experimental data from open-water operations. This model was then implemented in Simulink and a Bode analysis was performed on the open loop transfer functions. Once the desired phase margin crossover frequency was achieved, the system was run in Simulink to ensure the performance of the system met overshoot and stability requirements. Finally, the improved gains were tested in open water sea trials in Bedford Basin and the nearby open water. Both improved gain sets resulted in better performance that the original baseline gain set and have been demonstrated to meet the requirements for high quality Synthetic Aperture Sonar imagery and SeaVision™ 3D laser imaging. These control system improvements have since been implemented on systems worldwide as part of Kraken Robotic Systems' ongoing product support and operational improvements were realized immediately in the field.**

***Index Terms*—3 DOF, control systems, Bode analysis, dynamic model, PID control, towfish, transfer function, unmanned underwater vehicles**

I. Introduction

Unmanned underwater vehicles (UUVs) have enabled underwater surveying [1], inspections [2] [3], and subseabed imaging [4] to be performed remotely, reliably, cost-effectively, and safely without the need for human intervention. Towing UUVs behind a surface vessel can increase their area coverage rate while also transmitting mission progress across the towing cable in real time. However, this introduces complex dynamics that must be taken into account [5] [6]. This paper examines the modeling, development, testing, and real-world implementation of a control scheme on the Kraken KATFISH™ vehicle, a high speed, actively stabilized Synthetic Aperture Sonar (SAS) towed UUV used for underwater survey work throughout the world [7]. An image of the KATFISH™ can be seen in Fig. 1. In this paper, controller development takes place in three steps: development of a dynamic model, development of a control scheme, and live survey testing.

SAS has tight performance requirements, necessitating a high performance controller. The control scheme implemented on this vehicle utilized a three degree of freedom (DOF) proportional–integral–derivative (PID) controller. A PID controller is a very common control scheme for underwater vehicles and is used in several works such as [8], [9], and [10].

Fig. 1. Two KATFISH™ vehicles awaiting deployment.

Once the response of the uncontrolled system was modelled, the effect of the PID gains was assessed using a Bode analysis. The analysis was focused on the phase margin and crossover frequency. Several gain sets were tested during seatrials and then refined to create a stable, responsive system.

Here, the methods used for modeling the KATFISH™ vehicle are discussed in Section II. The Bode and simulation analysis are discussed in Section III and the seatrial tests are discussed in Section IV. Finally, the conclusions are discussed in Section V.

II. Modeling

The dynamic response of the KATFISH™ vehicle was modeled using data from trials undertaken in Bedford Basin, Nova Scotia in September 2020. This series of trials was recommended by previous work performed at Kraken Robotic Systems [11]. With the data provided by this series of trials, linear regression was used to find the best-fit approximation of the vehicle's open loop response to a step input command using the following equation:

$$b = A * x \tag{1}$$

Here, b and A were known matrices and linear regression was used to solve for x. The x vector contained the coefficients

of the Laplace space transfer functions representing the system dynamics, K and τ, described in Eq. 2 through 4. The time delay for the servo response was also determined using the KATFISH™ data by comparing the difference between the time a command was issued by the control system and the time a response in the control system was observed.

The roll tests comprised 20 step inputs that varied from approximately ±20° to ±35°. In these tests, vehicle speeds varied from 2.55 m/s (5.0 kts) to 4.97 m/s (9.7 kts) and utilized cable scopes of 28.43 m to 250 m. For this axis, the input variable, b, was set equal to the roll angle, ϕ, and the output variable, A, was set to $\begin{bmatrix}-\dot{\phi} & Moment_x\end{bmatrix}$. To account for the use of the angle itself rather than the derivative in the A vector, an extra derivative was taken in the transfer function. This results in a transfer function with the form:

$$\frac{Y(s)}{U(s)} = \frac{Ks}{\tau s + 1} \tag{2}$$

The focus of the least squares analysis was on the step rise or fall, depending on direction. For the roll axis, a time window of 4 seconds was used.

The pitch tests consisted of 18 step inputs that varied from approximately ±5° to ±15° with vehicle speeds of 2.54 m/s (4.9 kts) to 5.02 m/s (9.8 kts) and cable scopes of 28.43 m to 250 m. The input variable, b, was set to equal the pitch angular velocity, ω_y, and the output variable, A, was set equal to $\begin{bmatrix}-\dot{\omega}_y & Moment_y\end{bmatrix}$. For the pitch axis, a time frame of 2 seconds centered on the step rise (or fall) was chosen as a best-fit for the data. For this axis, the transfer function had the form:

$$\frac{Y(s)}{U(s)} = \frac{K}{\tau s + 1} \tag{3}$$

For this axis, an additional metric was introduced: the principal moment of inertia about the y-axis. This metric was calculated for each transfer function using the following equation:

$$I_p = \frac{\tau}{K} \cdot \frac{180}{\pi} \tag{4}$$

The resulting value was then compared to the vehicle configuration value. This provided a second method to check the accuracy of the best-fit time frame. A time frame that resulted in a close match was assumed to more accurately reflect the vehicle behavior.

The yaw tests featured 20 step inputs that ranged from approximately ±5° to ±20°. The vehicle speeds varied from 2.19 m/s (4.3 kts) to 4.96 m/s (9.6 kts) and featured cable scopes of 28.43 m to 250 m. Note that these tests are more heavily weighted to negative step inputs and that the formulation for the yaw axis used Eq. 3. The input variable, b, was set equal to the yaw angular velocity, ω_z, and the output variable, A, was set equal to $\begin{bmatrix}-\dot{\omega}_z & Moment_z\end{bmatrix}$. Here, the best-fit time frame was chosen to be 2.5 seconds centered on the step rise or fall. Again, the principal moment of inertia about the z-axis was used as a second metric for determining the best-fit time frame. Eq. 4 was used to calculate this value which was then compared to the vehicle configuration value.

Once all the transfer functions were calculated, a nominal, or best-representative, transfer function was selected for each of the three axes. These transfer functions were selected based on three criteria:

- Use of mid-range cable scope as this best represents nominal operating conditions.
- Use of mid-range velocity as this best represents nominal operating conditions.
- Transfer function exhibits a good fit of the experimental data.

The nominal transfer functions were found to be a good fit for the data because they resulted in the lowest least-squares value. The form of these transfer functions can be seen in Table I.

In addition to these nominal transfer functions, three additional transfer functions were needed for a complete model of the system:

- Pitch angle to depth
- Depth to measured depth
- Commanded fin deflection angle to actual fin deflection angle

These additional transfer functions used in the work presented here are reproduced from [11] for reference in Table II.

Finally, the estimate of a 13 ms time lag between servo commands and responses found in [11] was verified by looking at the time stamp differences between the issued servo command and the first observed servo response. This time lag was considered in both the numerical analysis and in the Simulink models, both of which will be discussed further in the next sections.

III. Bode and Simulation Analysis

The system analysis was performed in two parts: a Bode analysis and a Matlab Simulink simulation. The Bode analysis was performed in Matlab R2021a using the Control System Toolbox. This allowed for the examination of phase margin, crossover frequency, and inner and outer loop stability before testing in Simulink. Simulink modeled the KATFISH™ dynamics and PID control scheme to create a closed-loop simulation that allowed for a more complete visualization of the resultant control. This also allowed for the consideration of overshoot, which needed to be kept to a reasonable level. Several internal options for rate limiting were also modified to better align with the system performance during this step. The improved rates further improved vehicle responsiveness and stability.

The first axis examined in simulation was the roll axis, which is controlled by the roll controller. This controller is almost always commanded to a maintain a value of 0° and consists of inner loop and outer loop PID controllers. The original gains can be seen in Table III while the corresponding phase margin and crossover frequency can be seen in Table IV.

Input Variable (symbol, unit)	Output Variable (symbol, unit)	Transfer Function
Moment about the X axis (M_x, Nm)	Roll Angle (ϕ, degrees)	$\frac{\omega_x(s)}{M_x(s)}$
Moment about the Y axis (M_y, Nm)	Pitch Angular Velocity (ω_y, degrees/second)	$\frac{\omega_y(s)}{M_y(s)}$
Moment about the Z axis (M_z, Nm)	Heading Angular Velocity (ω_z, degrees/second)	$\frac{\omega_z(s)}{M_z(s)}$

TABLE I
KATFISH™ TRANSFER FUNCTIONS CALCULATED FROM THE SEPTEMBER 2020 CONTROLS TRIAL DATA.

Input Variable (symbol, unit)	Output Variable (symbol, unit)	Transfer Function
Pitch Angle (θ, degrees)	Depth (d, m)	$\frac{d(s)}{\theta(s)}$
Depth (d, m)	Measured Depth ($\hat{d}$, m)	$\frac{\hat{d}(s)}{d(s)}$
Commanded Fin Deflection Angle (u, degrees)	Fin Deflection Angle (δ, degrees)	$\frac{\hat{\delta}(s)}{u(s)}$

TABLE II
ADDITIONAL KATFISH™ SYSTEM TRANSFER FUNCTIONS REPRODUCED FROM [11].

Note that the inner loop characteristics are not defined for the baseline gains in Table IV. This is because the roll inner loop does not reach its target step value of 1 with the original gains as shown in Fig. 2. Thus, the inner loop proportional gain was increased significantly in order to compensate for this disparity. The original outer loop gains also demonstrated a slow response time of over 100 seconds to reach the target step value of 1 in the outer loop response shown in Fig 2. This slow response is confirmed by the low outer loop crossover frequency of 0.05 rad/s. Thus, the crossover frequency was also significantly increased for the outer loop gains so that the KATFISH™ could correct for roll disturbances in a timely manner.

In order to achieve the desired level of stability, the phase margin for the roll was kept between 60° and 100°. Since one of the biggest concerns about the roll controller was its extremely slow response time, the crossover frequency was increased while maintaining the desired level of stability. Through experimentation, it was found that underdamped systems met all the desired criteria. The result of these changes in the gain set is shown in Table III. A comparison of the step responses in Fig. 2 reveals that the improved gain set is much more responsive than the original data set. Further, there is no oscillation in either gain set. This is verified by the results from Simulink, shown in Fig. 3. This simulation resulted in a rise time of approximately 2 s and an overshoot of 0.05°. This was well within the desired performance criteria.

The pitch axis controllers were examined next. Note that there are two pitch axis controllers for the KATFISH™ vehicle: the pitch controller, which directly controls the pitch axis and the depth controller, which controls both depth and altitude modes. Both controllers consist of inner and outer loop PID controllers and, in fact, share the same inner loop. For this reason, the inner loop gains were modified to match since they control the same physical system. The original gains can be seen in Table V while the corresponding phase margin and crossover frequencies can be seen in Table VI.

In the original baseline gain sets, both the pitch and depth inner loops have higher than recommended phase margins. A jog is seen on the inner loop plots in both Fig. 4 and Fig. 5 as a result of this high phase margin. Thus, the phase margin was lowered to within the recommended bounds of 60° and 100° mentioned above. In addition, the crossover frequency for the original inner pitch loop is too low, as seen in the long rise time of 30 seconds illustrated in Fig. 4. This value was also raised. Finally, both original outer loops are underdamped, especially the depth outer loop, so the damping for both loops was increased.

The pitch and depth gains, phase margins, and crossover frequencies for both the original baseline and improved gain sets can be seen in Table V and VI. Note that the crossover frequency was not changed for the depth outer loop because the response time is largely limited by pitch angle. Larger crossover frequencies require a larger pitch angle to achieve which would affect the quality of the SAS data. Thus, the depth outer loop is limited in term of responsiveness. However, since the vehicle spends most of its time maintaining depth rather than reaching depth, this was not deemed to be an area of concern. The improved performance achieved by these gain sets was verified by Simulink, as shown in Fig. 6 and 7. Here, it can be seen that the pitch exhibited a rise time of approximately 1 s and an overshoot of 0.20° while the depth had a rise time of about 19 s and an overshoot of 0.07 m.

The final axis examined was the yaw axis. This controller consists of inner and outer loop PID controllers. The original baseline gains for this loop can be seen in Table VII and their corresponding phase margin and crossover frequencies can be seen in Table VIII.

The yaw inner loop had a higher than recommended phase margin and the effect of this can be seen as a jog early in the step response plot shown in Fig. 8. Thus, the phase margin was lowered to within the recommended bounds. The crossover frequency was also lower than desired and was increased in order to create a more stable, responsive system. The original outer loop is underdamped and was modified to have a little more proportional gain. In addition, the crossover frequency, while acceptable in and of itself, was higher than the inner loop crossover frequency. This should not happen in a stable system as it forces the outer loop to update before the inner loop. This was also addressed by the improved gain set.

The gains, phase margins, and crossover frequencies for the original baseline gains and the improved gains can see seen

Controller Name	Receives Commands	Input Variable	Output Variable	Proportional Gain	Integral Gain	Derivative Gain
Roll Inner Loop (Original)	Roll Outer Loop	Roll Rate (degrees/second)	Roll Moment Command (Nm)	0.4	0.6	0.2
Roll Outer Loop (Original)	User	Roll Angle (degrees)	Roll Rate Command (degrees/second)	0.3	0	0
Roll Inner Loop (Improved)	Roll Outer Loop	Roll Rate (degrees/second)	Roll Moment Command (Nm)	1.5	30	0
Roll Outer Loop (Improved)	User	Roll Angle (degrees)	Roll Rate Command (degrees/second)	3	0	0

TABLE III
ROLL AXIS CONTROLLER WITH THE ORIGINAL BASELINE AND IMPROVED GAINS.

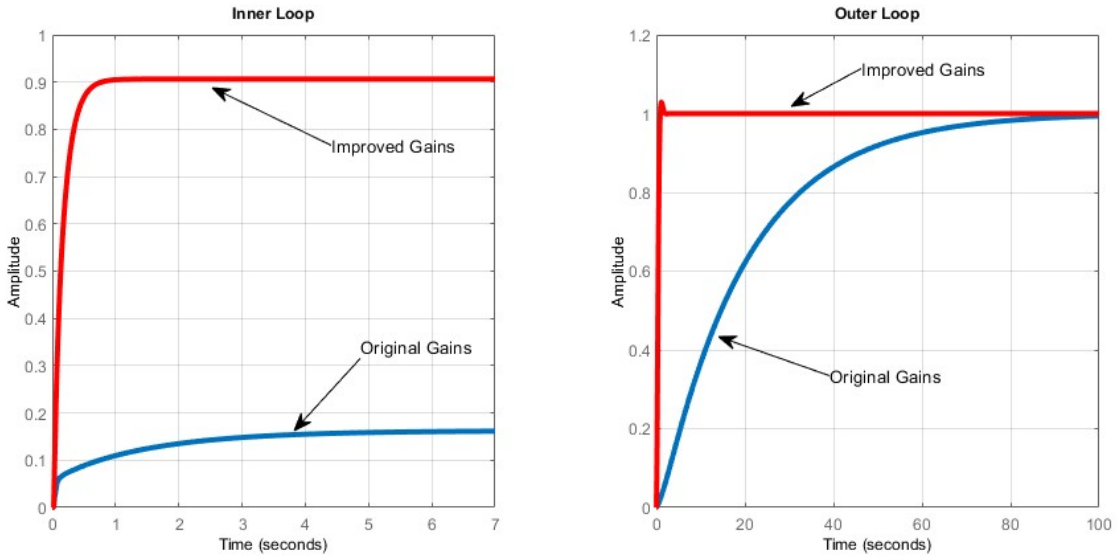

Fig. 2. Step responses from simulation for the roll gains.

Controller Name	Phase Margin (degrees)	Crossover Frequency (radians/second)
Roll Inner Loop (Original)	Inf	NaN
Roll Outer Loop (Original)	87.3	0.05
Roll Inner Loop (Improved)	91.5	5.49
Roll Outer Loop (Improved)	66.7	2.53

TABLE IV
ORIGINAL AND IMPROVED ROLL AXIS CONTROLLER BODE CHARACTERISTICS.

in Tables VII and VIII. The result of the Simulink verification can be seen in Fig. 9. The yaw was revealed to have a rise time of about 7 s and an overshoot of about 0.02°. This represents a significant improvement over the original baseline gain set.

IV. PHYSICAL TESTING

Next, the gains and rates were tested in seatrials where the KATFISH™ vehicle was taken into open water near Dartmouth, Nova Scotia, launched, and flown at a constant speed of approximately 7 kts for a series of lines. In each line, the vehicle was issued the following command sequence twice: a step down for each control variable (roll, pitch, depth, and yaw) followed by a step up for each control variable. This test was repeated for each set of gains and for each control variable. Once testing was complete, the collected data and user feedback was analysed to determine the vehicle performance. When necessary, the gain sets were modified and tested again. An example of the plots produced during seatrails can be seen in Fig. 10.

A roll step response during seatrials for both the original baseline and the improved gain sets can be seen in Fig. 11. The original baseline gain set did not reach its target value in over

Controller Name	Receives Commands	Input Variable	Output Variable	Proportional Gain	Integral Gain	Derivative Gain
Pitch Inner Loop (Original)	Pitch Outer Loop	Pitch Rate (degrees/second)	Pitch Moment Command (Nm)	30	10	0
Pitch Outer Loop (Original)	User	Pitch Angle (degrees)	Pitch Rate Command (degrees/second)	0.5	0	0
Pitch Inner Loop (Improved)	Pitch Outer Loop	Pitch Rate (degrees/second)	Pitch Moment Command (Nm)	25	150	0
Pitch Outer Loop (Improved)	User	Pitch Angle (degrees)	Pitch Rate Command (degrees/second)	3	0	0
Depth Inner Loop (Original)	Depth Outer Loop	Depth Rate (degrees/second)	Depth Moment Command (Nm)	40	40	5
Depth Outer Loop (Original)	User	Depth Angle (degrees)	Depth Rate Command (degrees/second)	0.5	0	0.6
Depth Inner Loop (Improved)	Depth Outer Loop	Depth Rate (degrees/second)	Depth Moment Command (Nm)	25	150	0
Depth Outer Loop (Improved)	User	Depth Angle (degrees)	Depth Rate Command (degrees/second)	1	0	7

TABLE V
PITCH AXIS CONTROLLERS WITH THE ORIGINAL BASELINE AND IMPROVED GAINS.

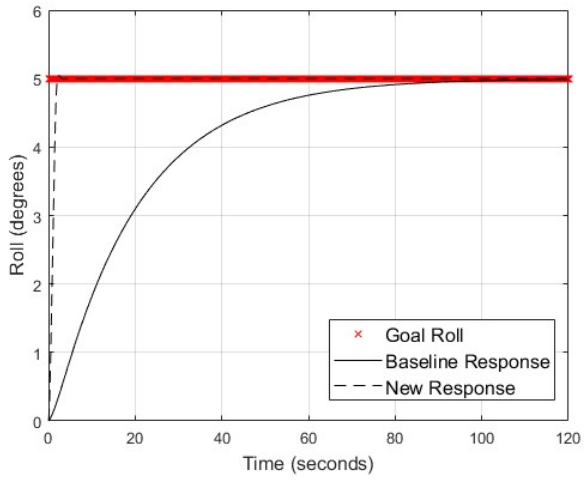

Fig. 3. Roll performance comparison in Simulink.

Controller Name	Phase Margin (degrees)	Crossover Frequency (radians/second)
Pitch Inner Loop (Original)	147.4	0.70
Pitch Outer Loop (Original)	68.7	0.31
Pitch Inner Loop (Improved)	81.8	5.01
Pitch Outer Loop (Improved)	59.8	2.67
Depth Inner Loop (Original)	130.7	2.67
Depth Outer Loop (Original)	5.7	0.14
Depth Inner Loop (Improved)	81.8	5.01
Depth Outer Loop (Improved)	68.5	0.13

TABLE VI
ORIGINAL AND IMPROVED PITCH AXIS CONTROLLERS BODE CHARACTERISTICS.

90 s of testing. The improved gain set, however, reached the same target value with a rise time of 1.26 s and an overshoot of 0.35°, which is very close to the values predicted in simulation. The steady state standard deviation of the seatrial step response was 0.08°, resulting in a very stable platform.

The seatrial pitch step responses can be seen in Fig. 12 for both the original baseline and improved gain sets. Using the original baseline gains, the target value was reached with a rise time of 5.50 s and an overshoot of 0.86°. The step response featured a steady state standard deviation of 0.32°. With the improved gains, the same target value was reached with a rise time of 0.50 s, an order of magnitude more responsive than the original system. The improved gain set also featured an overshoot of 0.35° and a steady state standard deviation of 0.08°. These values also represent a significant improvement over the original baseline gain set, resulting in a more responsive platform.

The depth responses can be seen in Fig. 13. The original baseline gains reached the target value with a rise time

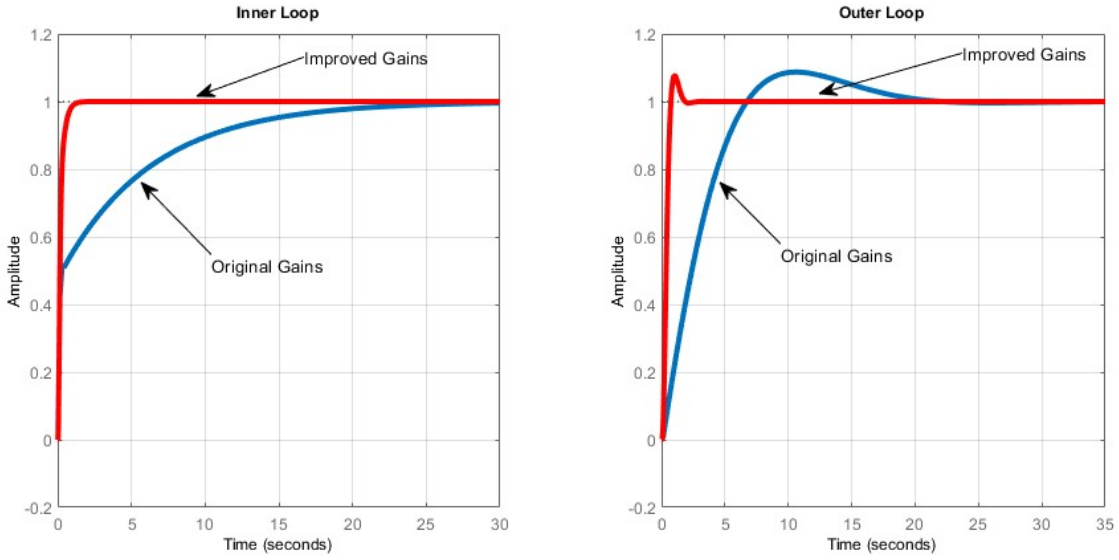

Fig. 4. Step responses from simulation for the pitch gains.

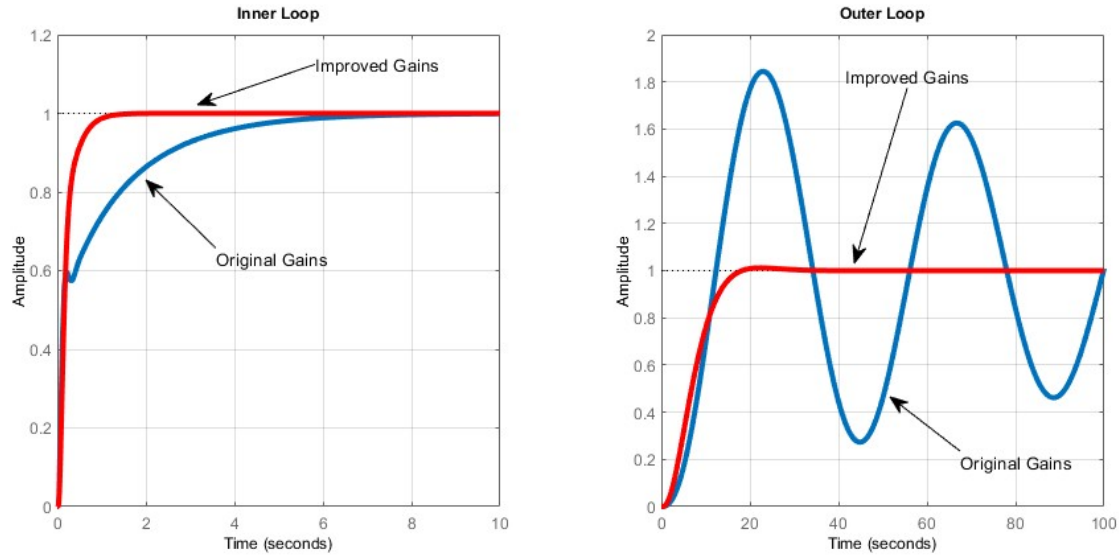

Fig. 5. Step responses from simulation for the depth gains.

of 18.54 s and an overshoot of 0.93 m. The steady state standard deviation was 0.14 m. However, it also failed to settle and oscillated continuously about the steady state value. In contrast, the improved gain set did settle about its target value. The target value was reached with a similar rise time of 19.62 s and a much improved overshoot of 0.01 m. It then maintained a steady state standard deviation of 0.02 m. Since this axis is crucial for SAS data collection, the improved system performance and stability was most apparent here.

Finally, the yaw seatrial step responses can be seen in Fig. 14. The original baseline gains reached the target value in 13.92 s with an overshoot of 0.20°. The steady state standard deviation for this data set was 0.16°. Once again, the improved gain set reached the same target value an order of magnitude faster with a rise time of 1.46 s. However, the improved gain set did result in a doubled overshoot of 0.40°. This was still well within accepted bounds. The improved gain set also featured a much lower steady state standard deviation of 0.03°, resulting in a much more stable platform.

Controller Name	Receives Commands	Input Variable	Output Variable	Proportional Gain	Integral Gain	Derivative Gain
Yaw Inner Loop (Original)	Yaw Outer Loop	Yaw Rate (degrees/second)	Yaw Moment Command (Nm)	10	5	0
Yaw Outer Loop (Original)	User	Yaw Angle (degrees)	Yaw Rate Command (degrees/second)	0.6	0	0
Yaw Inner Loop (Improved)	Yaw Outer Loop	Yaw Rate (degrees/second)	Yaw Moment Command (Nm)	25	150	0
Yaw Outer Loop (Improved)	User	Yaw Angle (degrees)	Yaw Rate Command (degrees/second)	3	0	0

TABLE VII
YAW AXIS CONTROLLER WITH THE ORIGINAL BASELINE AND IMPROVED GAINS.

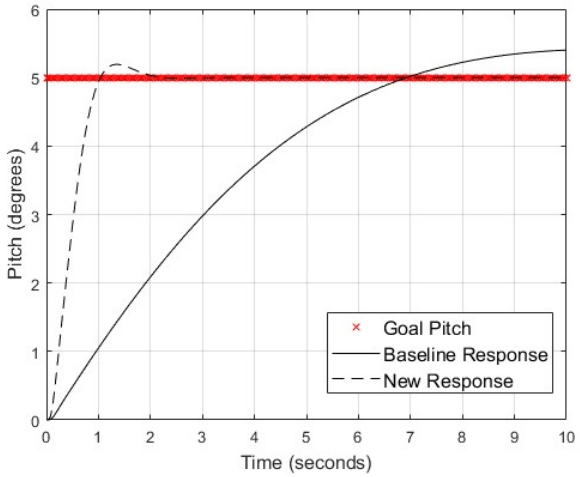

Fig. 6. Pitch performance comparison in Simulink.

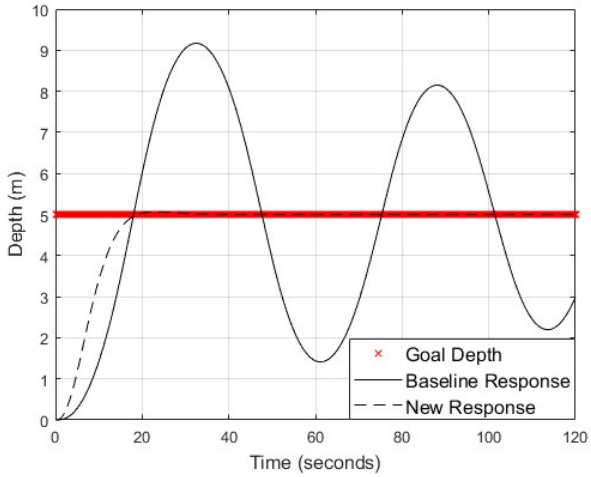

Fig. 7. Depth performance comparison in Simulink.

Controller Name	Phase Margin (degrees)	Crossover Frequency (radians/second)
Yaw Inner Loop (Original)	106.1	0.16
Yaw Outer Loop (Original)	50.0	0.27
Yaw Inner Loop (Improved)	76.5	4.79
Yaw Outer Loop (Improved)	58.1	2.74

TABLE VIII
ORIGINAL AND IMPROVED YAW AXIS CONTROLLER BODE CHARACTERISTICS.

V. CONCLUSIONS

Although the original baseline gain set was adequate for the KATFISH™ control system, the towbody control response time was significantly decreased by increasing the system gains. Proper gain selection was performed with the help of traditional tools expedited with MATLAB and Simulink. Analysis suggested that a few simple changes to the PID gains would result in a much more stable and responsive system. Various gain sets were developed to achieve this goal using newly developed system mathematical models and simulations. While multiple gain sets resulted in a better performing system than that displayed by the original baseline gains, the improved gain set was ultimately selected for deployment on the KATFISH™ vehicle. This resulted in a stable, responsive system that met all SAS vehicle requirements. The control system improvements were subsequently pushed to systems worldwide as part of Kraken Robotic Systems' ongoing product support, with operational improvements realized immediately in the field.

Another advantage of this method was that it resulted in fast turn around times for improved gain solutions and high confidence in the gain performance before use on the actual vehicle. This meant that operators did not have to worry about damaging the KATFISH™ due to risky experimentation and that future improvements could be tested and fielded quickly. Future work is planned to further reduce the development and testing time for the KATFISH™ platform. In addition, future work is planned to extend the control regime to speeds up to

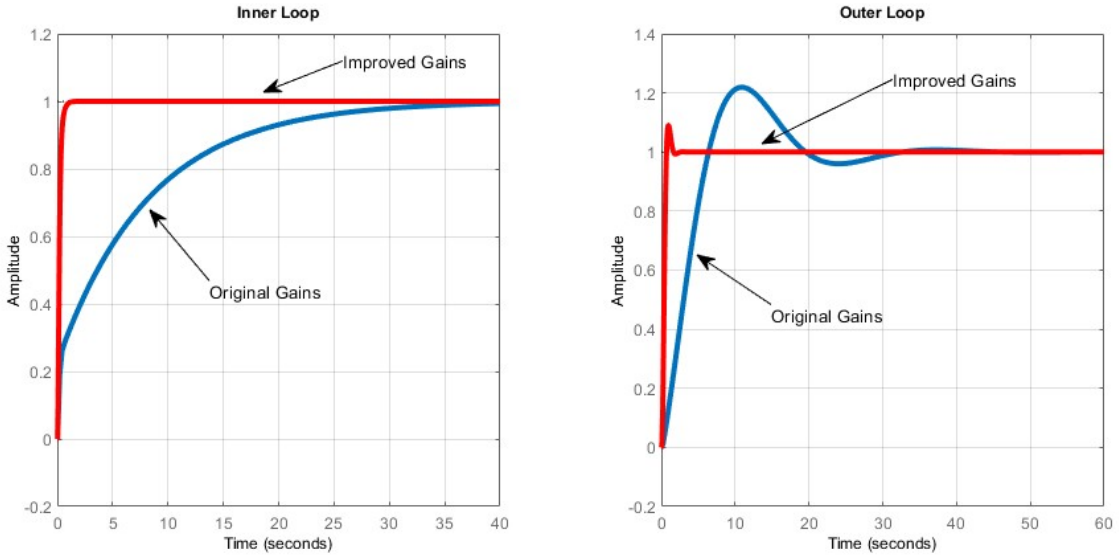

Fig. 8. Step responses from simulation for the yaw gains.

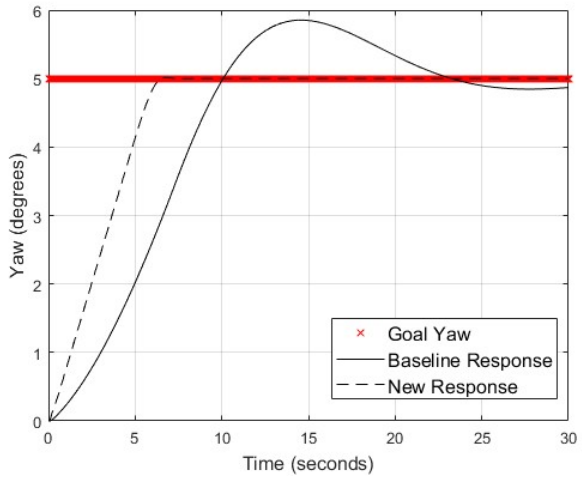

Fig. 9. Yaw performance comparison in Simulink.

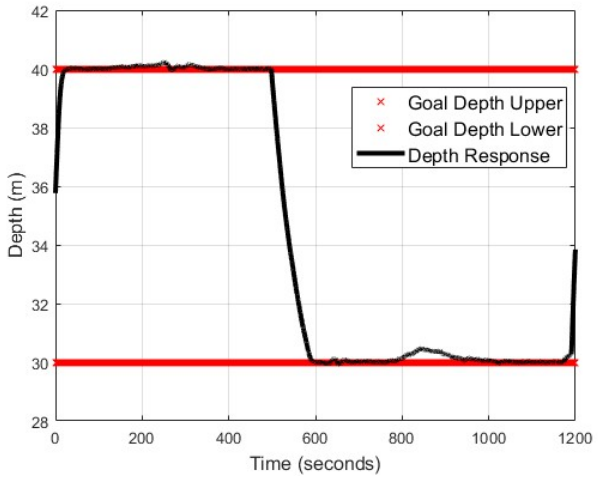

Fig. 10. An example of the depth plot using seatrial data.

10 kts. The analysis and simulation process discussed in this paper will aide in this effort.

REFERENCES

[1] J. D. Holmes, W. M. Carey, J. F. Lynch, A. E. Newhall, and A. Kukulya, "An autonomous underwater vehicle towed array for ocean acoustic measurements and inversions," in Europe Oceans, Brest, France, (2005).

[2] N. Kizor V, B. Shirose, M. Adak, M. Kumar, S. Jayandan J, A. Srinivasan, and R. S. MuhammadN, "Design of a Remotely Operated Vehicle (ROV) for Biofoul Cleaning and Inspection of Variety of Underwater Structures," in RSI International Conference on Robotics and Mechatronics, Tehran, Islamic Republic of Iran, (2021).

[3] M. S. B. M. Soberi, Z. H. Ismail, M. Z. B. Zakaria, and K. Sammut, "Autonomous ship hull inspection by omnidirectional path and view," in IEEE/OES Autonomous Underwater Vehicles, Tokyo, Japan, (2016).

[4] M. Gutowski, J. M. Bull, J. K. Dix, T. J. Henstock, P. Hogarth, T. Hiller, T. G. Leighton, and P. R. White, "3D high-resolution acoustic imaging of the sub-seabed", *Applied Acoustics*, Vol. 69, Issue 3, pp. 262-271 (2008).

[5] E. M. Schuch, A. C. Linklater, N. W. Lambeth, and C. A. Woolsey, "Design and Simulation of a Two Stage Towing System," in Proc. IEEE OCEANS, Washington, DC, USA, (2005).

[6] J. Huifeng, F. Wei, Z. Lindan, Z. Chuncheng, and Z. Zhiheng, "Simulation research and optimization design on towed system of manned submersible," in IEEE 8th International Conference on Underwater System Technology: Theory and Applications, Wuhan, China, (2018).

[7] "Towed SAS Vehicle: KATFISH™", [Online] Available: https://krakenrobotics.com/products/towed-vehicles/ [Accessed 12 December 2022].

[8] Q. Chen, T. Chen, and Y. Zhang, "Research of GA-based PID for AUV Motion Control", in Proc. IEEE International Conference on Mechatronics and Automation, Changchun, China, (2009).

[9] S. S. Mikhalevich, S. A. Baydali, F. Manenti, "Development of a tunable

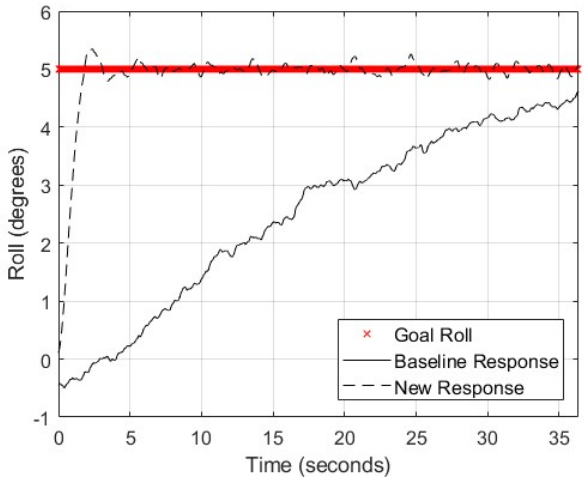

Fig. 11. Roll response comparison plot.

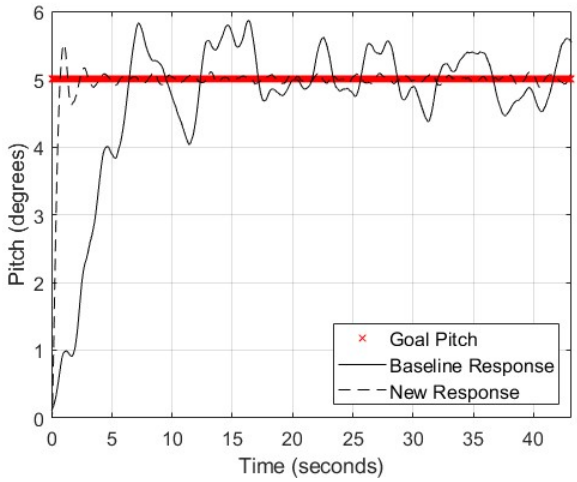

Fig. 12. Pitch response comparison plot.

method for PID controllers to achieve the desired phase margin", *Journal of Process Control*, Vol. 25, pp. 28-34 (2015).

[10] Y. Li, Y. Jiang, L. Wang, J. Cao, and G. Zhang, "Intelligent PID guidance control for AUV path tracking", *Journal of Central South University*, Vol. 22, pp. 3440–3449 (2015).

[11] A. Predmyrskyy "KATFISH™ Autopilot v2.1.0 Performance," Kraken Robotic Systems, Document: 92410002, Oct. 1, 2019.

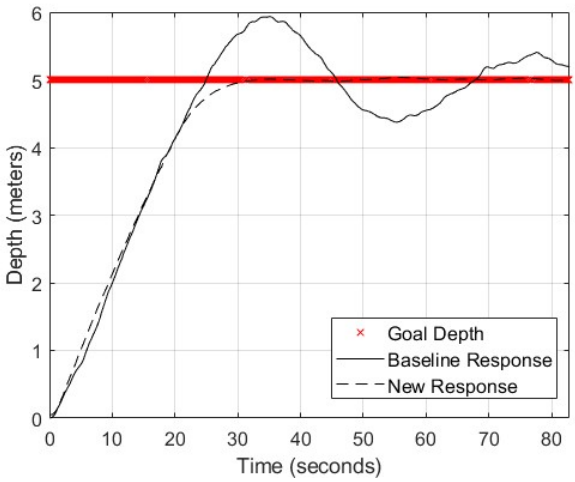

Fig. 13. Depth response comparison plot.

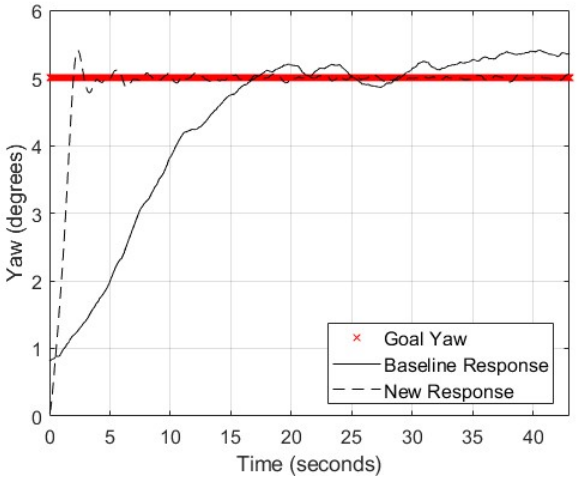

Fig. 14. Yaw response comparison plot.